In situ observation of the structure and dynamics of a polymer solution through nonsolvent-induced phase separation by x-ray photon correlation spectroscopy

Kazu Hirosawa [1,*] Tatsuhiro Iwama [1] Naoki Sakamoto,[1] Hiroyasu Masunaga,[2] and Taiki Hoshino [3,†]

[1]*Platform Laboratory for Science and Technology, Asahi Kasei Corporation, 2-1 Samejima, Fuji, Shizuoka 416-8501, Japan*

[2]*Japan Synchrotron Radiation Research Institute/SPring-8, 1-1-1, Kouto, Sayo-cho, Sayo-gun, Hyogo 679-5198, Japan*

[3]*International Center for Synchrotron Radiation Innovation Smart (SRIS) and Institute of Multidisciplinary Research for Advanced Materials (IMRAM), Tohoku University, 2-1-1 Katahira, Aoba-ku, Sendai 980-8577, Japan; and RIKEN SPring-8 Center, 1-1-1 Kouto, Sayo-cho, Say-gun, Hyogo 679-5148, Japan*

(Received 12 December 2022; revised 30 March 2023; accepted 6 April 2023; published 26 April 2023)

Nonsolvent-induced phase separation (NIPS) is a complex but important phenomenon involved in the manufacture of fibers and other polymeric industrial products. We performed *in situ* x-ray photon correlation spectroscopy (XPCS) measurements on a cuprammonium cellulose solution immersed in aqueous acetone solution to reveal the structure and dynamics involved in the NIPS process on the microscopic scale. A combination of the structural information from the small angle x-ray scattering profiles and the dynamic information from the XPCS analysis revealed that NIPS occurs via two steps: dilution of the polymer solution by the solvent and desorption of the solvent from the polymer solution. This study will provide an opportunity for the fundamental understanding of NIPS, which is important from both the scientific and industrial viewpoints.

DOI: 10.1103/PhysRevMaterials.7.045605

I. INTRODUCTION

Nonsolvent-induced phase separation (NIPS) involves the phase separation of a polymer solution induced by contact with a nonsolvent. NIPS is widely employed in fabrication processes of polymer materials, especially in the wet spinning of porous membranes and fibers [1,2]. In the wet spinning of porous membranes, the polymer solution is extruded in a form of a hollow fiber and is immediately immersed in a coagulation bath filled with nonsolvent; the porous structure is then formed via NIPS. For example, regenerated cellulose porous membranes for the application of virus filtration are manufactured by wet spinning of a cuprammonium cellulose solution in water or aqueous solutions of ketones [3–6]. The pore structure of the cellulose membranes can be controlled by altering the composition of the cuprammonium cellulose solution and the coagulation solution [6]. Manufacturers control the microstructures of membranes by optimizing the process conditions for the target products, but the optimization process is rather heuristic because of our limited understandings of NIPS.

Based on the classic Cahn-Hilliard theory for spinodal decomposition, NIPS processes are explained as follows: (i) the variation of the composition of the polymer solution by mutual diffusion of the solvent and nonsolvent, (ii) initiation of the spinodal decomposition and evolution of the amplitude of concentration fluctuation at a characteristic wavelength, and (iii) the coarsening of the spinodal structure, eventually resulting in macroscopic phase separation [7–9]. However, macroscopic phase separation is not achieved in actual wet spinning, and instead, microscopic porous structures are formed in the membranes. Such a contradiction comes from the lack of consideration to the composition-dependent mobility of the polymer. The mobility of the polymer decreases with increasing polymer fractions in the polymer-rich phase. Subsequently, the phase-separated structure is frozen in the way of the above-mentioned process (ii) or (iii). Thus, a microscopic porous structure is formed in the membranes as a nonequilibrium state [10,11]. In a recent study, the effects of the composition dependence of the mobility on the phase-separated structure was investigated by phase-field-based simulations [12,13]. Garcia *et al.* reported that a reduction in the mobility upon NIPS is essential for the formation of an asymmetric microscopic pore structure: The pore size gradually changes from the film-bath interface to the inner side of the film. Ishigami *et al.* investigated the kinetics of macroscopic solidification of polymer solutions in coagulation solutions by directly measuring the stiffness of the membrane [14]. However, few other experimental studies have focused on the solidification of NIPS. This is because of the difficulties in the *in situ* observation of solidification.

X-ray photon correlation spectroscopy (XPCS), which employs partially coherent x rays, allows microscopic observation from the temporal fluctuation of scattering intensity [15,16]. Using XPCS, various dynamic fluctuations in nonequilibrium systems have been studied on a wide range of timescales recently [17–24]. XPCS can be applicable to opaque samples, and phase-separated structures can be simultaneously characterized [25]. Such features are suitable for *in situ* investigations of the NIPS system. Recently, Girelli *et al.* studied the microscopic dynamics of temperature-induced liquid-liquid phase separation of a protein solution using

*hirosawa.kf@om.asahi-kasei.co.jp
†taiki.hoshino.c7@tohoku.ac.jp

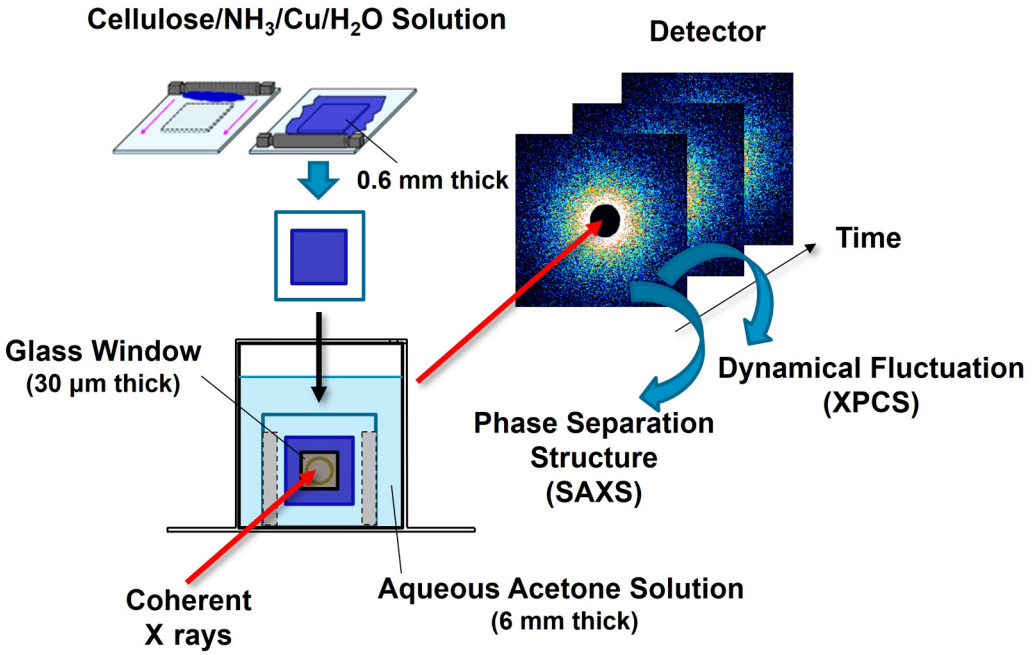

FIG. 1. Schematic illustration of the x-ray photon correlation spectroscopy (XPCS) measurement on the NIPS process of the cuprammonium cellulose solution (cellulose/NH_3/Cu/H_2O) in aqueous acetone solution.

in situ XPCS measurements and simulations [18]. The XPCS results showed a slowdown of dynamics in the late stage of the phase separation. The behavior was partially explained by the simulations based on Cahn-Hilliard theory considering mobility parameters. This shows that XPCS is a powerful method for *in situ* observation of solidification upon phase separation.

In this study, we carried out *in situ* XPCS measurements on NIPS of a cuprammonium cellulose solution in a coagulation solution. The changes in both the structure and dynamics upon phase separation were simultaneously investigated. Solidification was discussed in relation to the decrease in "velocity" of the dynamics. This is a report of *in situ* observation of the microscopic dynamics and structural growth in NIPS.

II. EXPERIMENT

NIPS proceeds when a polymer solution contacts a nonsolvent. As a polymer solution, we prepared a cuprammonium cellulose solution comprising cellulose/NH_3/Cu/H_2O, with a weight fraction of 0.06/0.048/0.020/0.872. The coagulation solution was diluted acetone (Fujifilm Wako Pure Chemical Co., Japan) with distilled water adjusted to a weight fraction of 0.30.

XPCS measurements were carried out at BL03XU, Spring-8 (Hyogo, Japan) [26]. The undulator source and Si(111) monochromator were tuned to an energy of 12.4 keV. The sample was irradiated with partially coherent x rays obtained by passing the beam through a pinhole 20 μm in diameter. The scattered x rays were detected using an Eiger 1M two-dimensional detector (Dectris, Switzerland). The sample to detector distance was approximately 8 m. Figure 1 shows the schematic illustration of the XPCS measurements. Using an applicator, a coating sample of the cuprammonium cellulose solution made on a 1 mm thick acrylic plate with a thickness of approximately 0.6 mm was prepared, and it was immediately (the lag time was 13 s) immersed in the coagulation bath and fixed to the wall on the x-ray axis with a plate spring. The thickness of the coagulation bath was 6 mm. The coagulation bath had 30 μm thick glass windows through which x rays entered, and scattered x rays could be extracted. XPCS measurements were started 34 s after the immersion, and the dynamics of the NIPS process was studied for approximately 10 min by repeating time-resolved measurements of 600 frames with an exposure time of 30 ms. During the measurement, the irradiation position was moved by 100 μm every 600 frames (irradiation time: 18 s) to avoid sample damage. The irradiation time at one position was determined by preliminary measurements.

III. RESULTS AND DISCUSSION

A. *In situ* observation of the phase-separated structure in NIPS

Structural changes in the cuprammonium cellulose solution under the NIPS process with an immersion time t_w can be discussed from the small angle scattering (SAXS) profiles, obtained by the circular average of the two-dimensional (2D) scattering images. At each irradiation position, every 100 frames (frames 1, 101, 201, 301, 401, and 501) were sampled and a circular average profile of each frame was obtained for SAXS analysis. Figure 2 shows the representative SAXS profiles $I(q)$ of the cuprammonium cellulose solution in the coagulation bath at various t_w values, with the scattering from the bath subtracted as background, where q is the scattering wave vector. With increasing t_w, the scattering intensity obviously increased. To discuss the dependence of the scattering intensity on t_w, invariant $Q \equiv (2\pi^2)^{-1} \int q^2 I(q) dq$ was calculated from the SAXS profiles in the range of $0.015\,\mathrm{nm}^{-1} < q < 0.10\,\mathrm{nm}^{-1}$, and the t_w dependence of Q is presented in

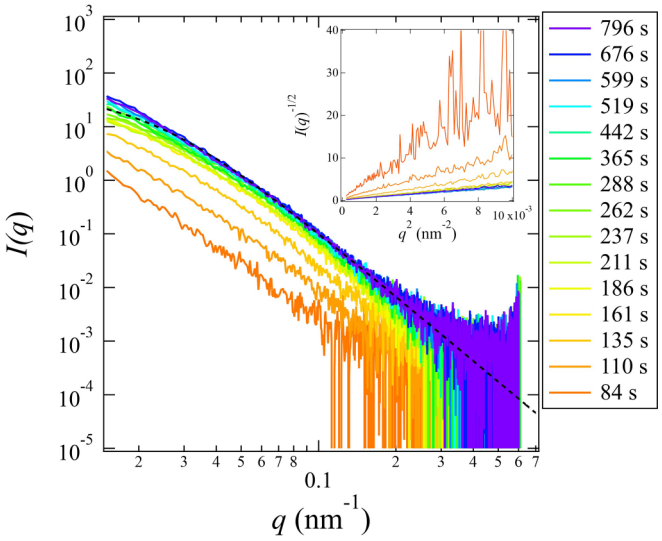

FIG. 2. Circular averaged SAXS profiles of the cuprammonium cellulose solution in coagulation bath at various immersion times. The dotted line shows the Debye-Bueche function, $I(q) = I_0/[1 + \Xi^2 q^2]^2$ with the correlation length, $\Xi = 45$ nm. The inset shows a plot in the form of $I(q)^{-1/2}$ vs q^2.

Fig. 3. Q drastically increased just after immersion through $t_w \approx 192$ s. In the ideal two-phase system, Q should be proportional to $\Delta\rho_e^2\varphi(1-\varphi)$, where $\Delta\rho_e$ is the difference in electron density between the two phases and φ is the volume fraction of a phase [27]. Considering that phase separation causes an increase in $\Delta\rho_e$ and/or φ, Q can be a measure of the progression of phase separation. The increase in Q observed on the present system implies that the cuprammonium cellulose solution went into the two-phase region just after immersion and the phase separation progressed until $t_w \approx 192$ s.

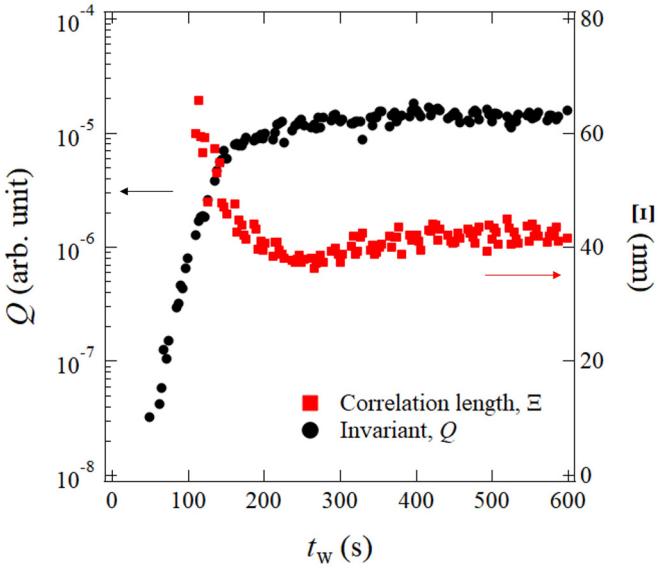

FIG. 3. Immersion time dependence of the invariant, $Q = (2\pi^2)^{-1} \int q^2 I(q) dq$ (black circles) and the correlation length, Ξ (red squares).

The SAXS profiles at $t_w > 110$ s were well reproduced by the Debye-Bueche (DB) function in the form of $I(q) = I_0/[1 + \Xi^2 q^2]^2$, where I_0 and Ξ are a constant value and correlation length, respectively, except for upturns in low q which are due to the small amount of aggregates. As a typical example, the curve in the DB function with $\Xi = 45$ nm is depicted by the dotted line in Fig. 2. Because the DB function is derived for an ideal two-phase system assuming that the phase boundary is sharp and the two phases are randomly intermixed [28,29], the fact that the SAXS profiles were well represented by the DB function indicates that phase-separated structures were formed in the solution on the microscopic scale. The inset of Fig. 2 shows the SAXS profiles in the form of $I^{-1/2}$ vs q^2. Based on the DB equation, Ξ can be evaluated from the slope in the range of $0.015\,\mathrm{nm}^{-1} < q < 0.10\,\mathrm{nm}^{-1}$ at $t_w > 84$ s. As shown in Fig. 3, Ξ clearly decreases at $t_w < 192$ s. In addition to classic theories of the spinodal decomposition [7–9], arrested spinodal decomposition of protein solutions forming colloidal gel have been intensely studied [30–32]. Moreover Tanaka has studied the effect of dynamic asymmetry on phase separation of polymer solutions and polymer blends [33–35]. The previous reports discussed domain coarsening and termination of structural growth by dynamical arrest in thermally induced phase separations (TIPS). However, the decrease of the correlation length with t_w, observed in our system, is not predicted from the previous reports. It is because of sequential variation of the system volume caused by interdiffusion of solvents. Phase separation by nucleation and growth takes place when the composition of the system is in a metastable region. However, the phase separation observed in the present system is assumed to be classified as spinodal decomposition rather than nucleation and growth for the following reasons. (i) In membranes prepared under conditions similar to the present system, a networklike morphology was observed instead of the particlelike morphology characteristic of nucleation/growth [4]. (ii) The mass transfer between the coagulation solution and the polymer solution occurs instantaneously, which is thought to cause the composition of the polymer solution to remain in a metastable region for a short time. Thus, we assume that the decrease in Ξ originated from shrinkage of the system caused by diffusion of the solvent from the polymer-rich phase into the coagulation solution. In the late stages of phase separation, both Ξ and Q became constant. The termination of the variation of Ξ and Q indicates a reduction in the mobility of the polymer upon phase separation. Here, it should be noted that Ξ and Q did not show discontinuous changes although they were obtained from different illumination spots (see Fig. S1 in the Supplemental Material [36]). This indicates that the NIPS process was successfully observed while avoiding the irradiation damage.

B. Dynamics

In the previous section, NIPS was discussed based on SAXS data. We suggested that the termination of phase separation was caused by a decrease in the mobility of the polymer. To confirm the hypothesis, the dynamic fluctuations of the phase-separated structure were investigated based on XPCS data.

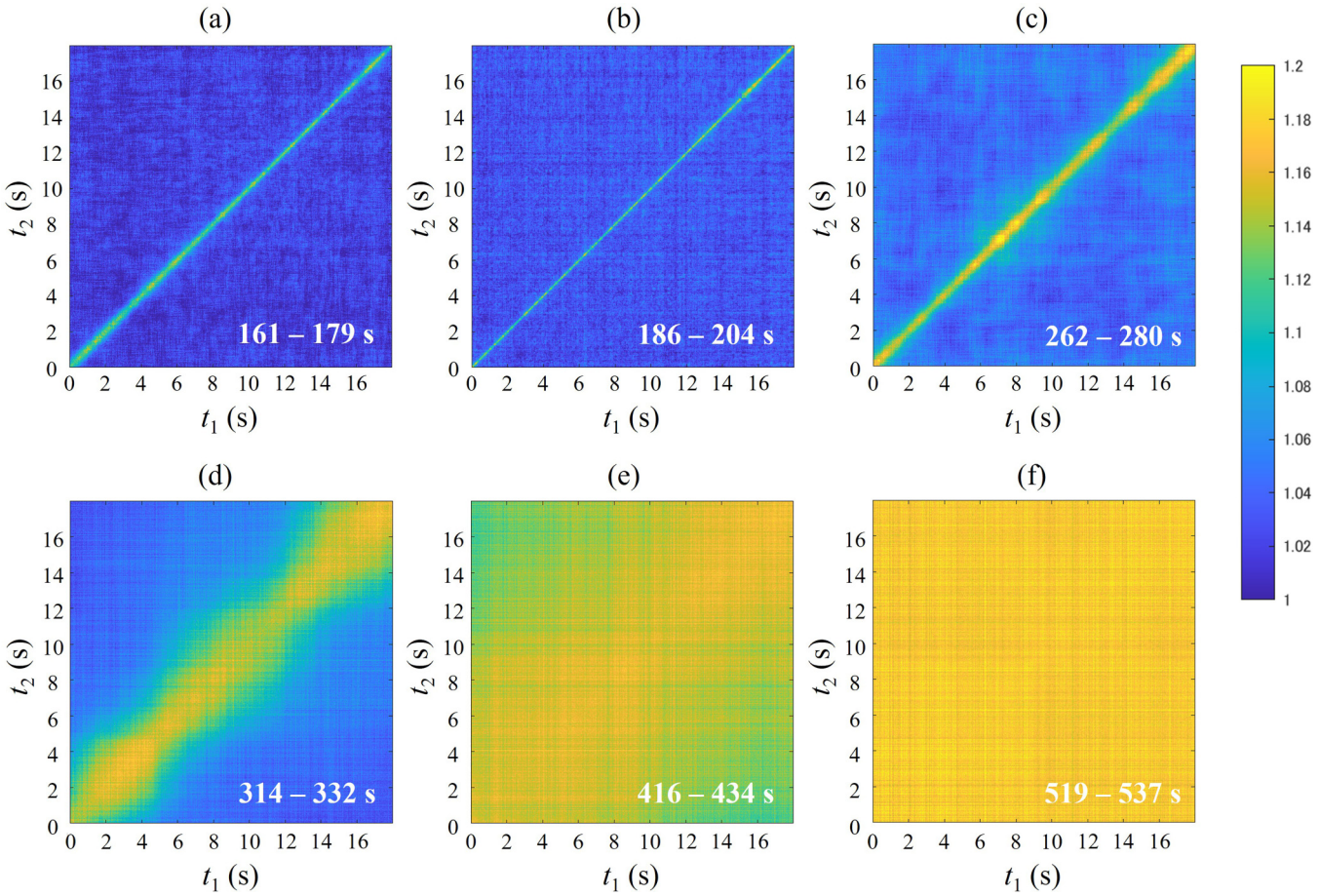

FIG. 4. Two-time correlation function C_I at $q = 0.0285\,\mathrm{nm}^{-1}$ at t_w = 161–179 s (a), 186–204 s (b), 262–280 s (c), 314–332 s (d), 416–434 s (e), and 519–537 s (f).

Here, we discuss the temporal variation of the dynamics via a two-time correlation function:

$$C_I(q, t_1, t_2) = \frac{\langle I_p(q, t_1) I_p(q, t_2)\rangle_\Psi}{\langle I_p(q, t_1)\rangle_\Psi \langle I_p(q, t_2)\rangle_\Psi}, \tag{1}$$

where $I_p(q, t)$ is the scattering intensity detected at a pixel at time t, and $\langle\cdots\rangle_\Psi$ denotes the average over pixels within $q \pm \Delta q$ [37,38]. The range of averaging, Δq, was set to $0.0015\,\mathrm{nm}^{-1}$, which was determined by considering the scattering intensity and the number of pixels. From C_I, the variation in the relaxation time can be represented visually by the width of the diagonal band [39]. The representative C_I at $q = 0.0285\,\mathrm{nm}^{-1}$ at various t_w values are shown in Fig. 4 (see all the obtained C_I at $q = 0.0285\,\mathrm{nm}^{-1}$ in Fig. S2 in the Supplemental Material [36]). As shown in Fig. 4(a), in the initial stage, the band is thinning with t_w, which means that the relaxation was becoming faster. Thereafter, as shown in Fig. 4(b), the relaxation starts slowing down from $t_w \approx 192$ s. Subsequently, the relaxation continues to slow down, eventually slowing down to exceed the measurement timescale, as shown in Figs. 4(c)–4(f).

For a more quantitative discussion, the temporal time-autocorrelation function was calculated from 100 frames (corresponding to 3 s) for $t_w < 240$ s and 600 frames (corresponding to 18 s) for $t_w > 240$ s, respectively, at various t_w, using the following formula:

$$g^{(2)}(q, \tau) = \frac{\langle\langle I_p(q, t) I_p(q, t+\tau)\rangle_\Psi\rangle_t}{\langle\langle I_p(q, t)\rangle_\Psi \langle I_p(q, t+\tau)\rangle_\Psi\rangle_t}, \tag{2}$$

where $\langle\cdots\rangle_t$ indicates time averaging. The obtained data were analyzed by fitting with the following equation:

$$g^{(2)}(q,\ \tau) = \beta \exp[-2(\Gamma\tau)^\alpha] + \text{baseline}, \tag{3}$$

where β, Γ, and α are the speckle contrast, relaxation rate, and compressed exponent, respectively. In the present measurements, t_w-independent $\beta \sim 0.12$–0.15 were obtained, which were similar to the measurements obtained from the different static samples with the same setup. Thus, although the previous studies have suggested that β has information on the relaxation being faster than the measured time window [40–42], it is not necessary to consider in this study. The value of α was between 1.0 and 2.0 and did not show systematic variation over time (see Fig. S3 in the Supplemental Material [36]). Due to the limited time range of the analysis caused by the t_w dependence of $g^{(2)}(q,\ \tau)$ and the presence of additional slow decay, the values of α were scattered, making it difficult to discuss them in detail.

Figure 5 shows the normalized time-autocorrelation functions, $[g^{(2)}(q,\ \tau) - \text{baseline}]/\beta$ at various t_w at $q = 0.0285\,\mathrm{nm}^{-1}$. Several $g^{(2)}(q,\ \tau)$ showed additional slower

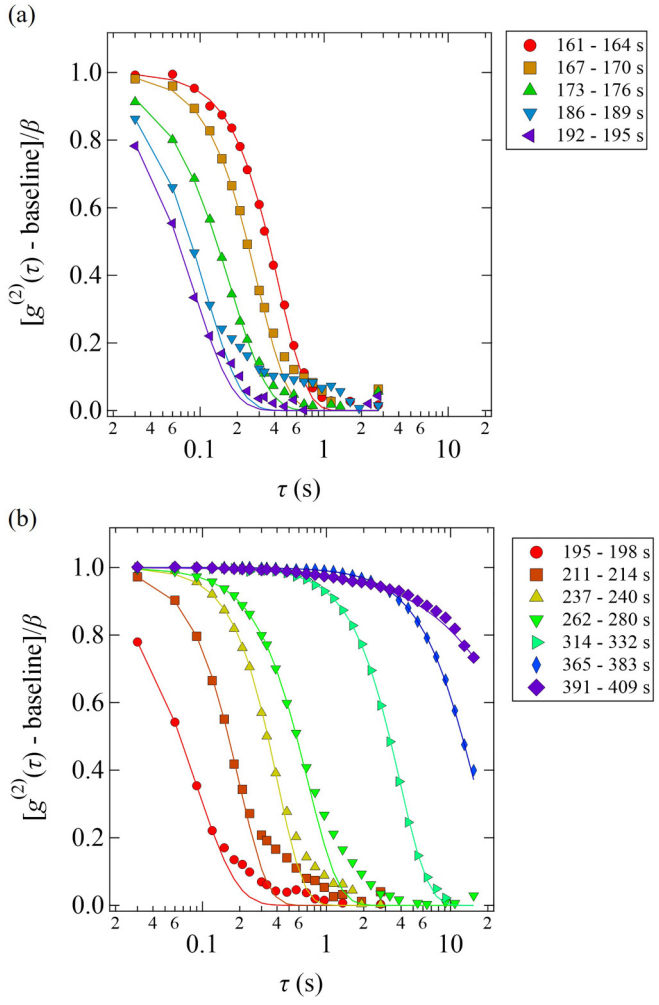

FIG. 5. Normalized time-correlation function of scattering intensity, $[g^{(2)}(\tau)$–baseline$]/\beta$ at $q = 0.0285\,\mathrm{nm}^{-1}$ in the range of (a) $t_w = 161$–192 s and (b) $t_w = 195$–409 s, respectively. The solid lines show the fitting curves by Eq. (3).

decay that behaved in a t_w-independent manner. Although the origin of the slower decay is not clear, we presume that it comes from a small amount of aggregate which separated from the membrane. We focused on faster decay as a main component to discuss phase separation. As mentioned in the discussion of C_I, in the time region of $t_w < 192$ s, $g^{(2)}(q,\ \tau)$ tends to relax faster with t_w as shown in Fig. 5(a), whereas in the time region of $t_w > 192$ s, $g^{(2)}(q,\ \tau)$ tends to relax slower with t_w as shown in Fig. 5(b). No significant time-autocorrelation functions were obtained for $t_w < 161$ s due to the low scattering intensity.

The obtained q dependences of Γ are shown in Fig. 6. As depicted by solid lines in Fig. 6, all measured Γ values were proportional to q, as expressed by $\Gamma \propto q^n$ $(n = 1)$, in the measured q range. The behavior of n and α differ from the characteristics of simple Brownian motion, i.e., $n = 2$ and $\alpha = 1$. This indicates that the observed dynamics of the phase-separated structure cannot be attributed to simple diffusive motion and rather are attributed to ballistic or hyperdiffusive motion [17]. The behavior of $n = 1$ and $\alpha > 1$ has been observed in XPCS analysis for several soft matter systems such as polymer grafted nanoparticle system [24,43], and filler particles dispersed in rubbers [44] and in a physical gel [45]. Although there is no clear consensus regarding the microscopic origin for the behavior, a shared feature of the systems is that the fluctuation accompanies some elastic deformations and stress relaxation [17,18]. In the present system, fluctuation in the phase-separated structure is affected by viscoelastic properties of the polymer-rich phase. It is assumed that such an effect of the viscoelasticity resulted in ballistic or hyperdiffusive behavior of the dynamics.

From the results of $\Gamma \propto q$, the "velocity" of the observed dynamics can be characterized by $v = \Gamma/q$. In Fig. 7, the t_w dependence of v is shown. At $t_w < 194$ s, v dramatically increases, showing a sharp peak at $t_w = 194$ s, followed by a drastic decrease at $194\ \mathrm{s} < t_w < 310$ s. Beyond $t_w = 310$ s, v becomes smaller over the measurement time range. To understand how these dynamic changes are related to the

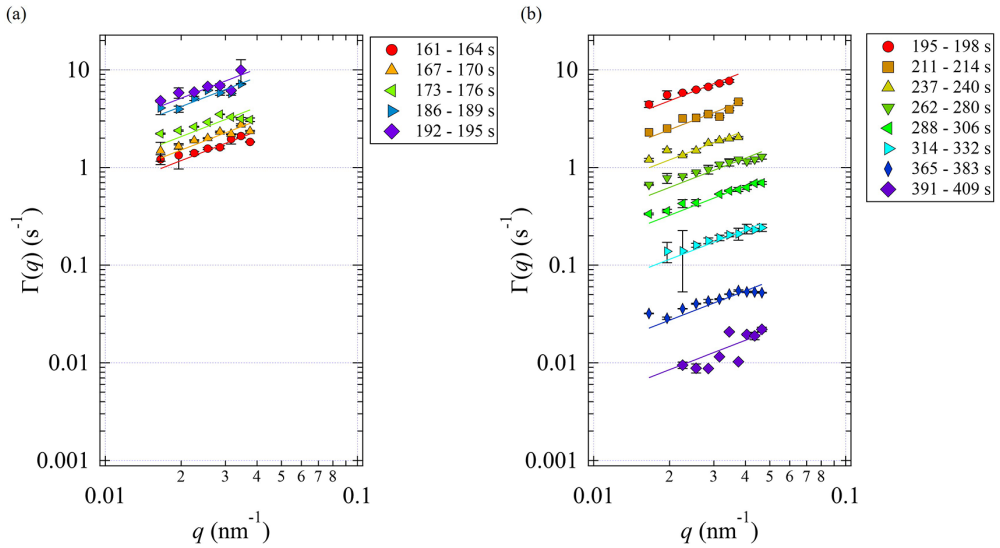

FIG. 6. Γ at various immersion times obtained from the curve fitting analysis on $g^{(2)}(\tau)$ by Eq. (3) in the range of (a) $t_w = 161-192$ s and (b) $t_w = 195-409$ s, respectively. The solid lines show fitting lines by $\Gamma = vq$.

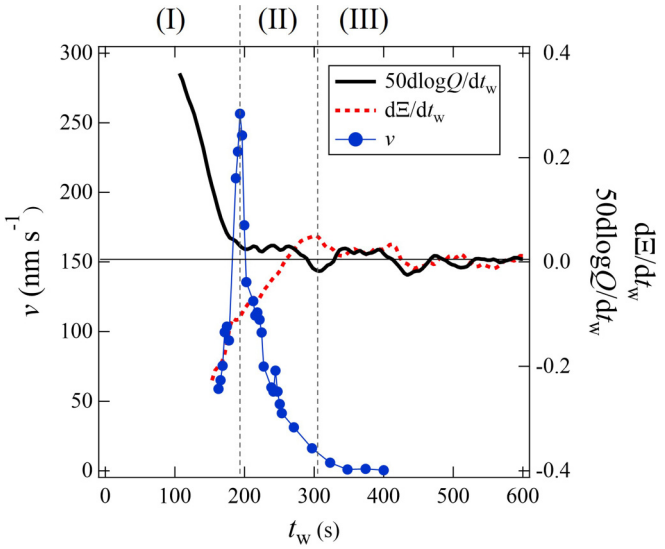

FIG. 7. Time dependence of $v = \Gamma/q$ with a dimension of velocity (blue filled circles). Time dependences of the derivative of the correlation length, Ξ, and the common logarithm of invariant, Q, are also shown as the black solid line and red dashed line, respectively.

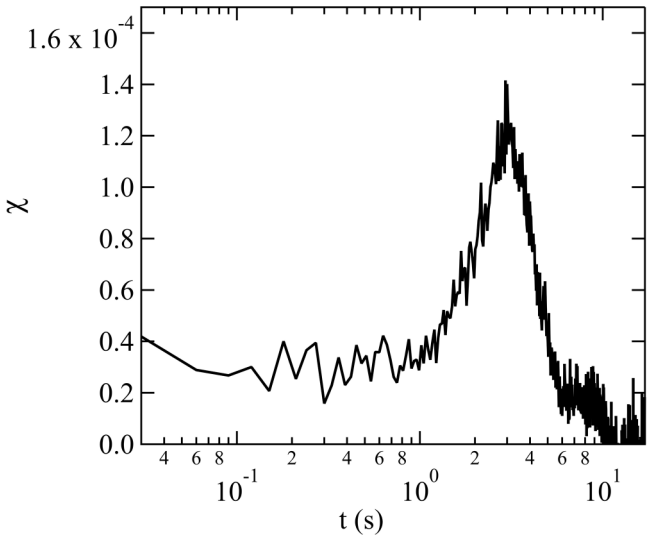

FIG. 8. χ, the fluctuation of C_I calculated from Eq. (4), at $q = 0.0285\,\mathrm{nm}^{-1}$ at $t_w = 314$–332 s.

static structure changes discussed in the previous section, differential functions with respect to t_w of the correlation length, $d\Xi/d\,t_w$, and the common logarithm of the invariant, $d[\log(Q)]/dt_w$, which was calculated by numerical differentiation after smoothing Ξ of the data in Fig. 3, are plotted in Fig. 7.

From the behavior of these parameters, the NIPS process can be divided into three stages: an initial stage (I), a second stage (II), and a last stage (III) as shown in Fig. 7. In stage (I), $d[\log(Q)]/dt_w$ has a clearly positive value, which implies that the phase separation progressed in the polymer-rich membrane (cuprammonium cellulose solution) by absorbing solvents (aqueous acetone solution). However, the SAXS profiles did not show a characteristic shoulder in the stage, indicating that the phase-separated structure was still not clear. During this process the polymer solution was diluted by solvents. It enhanced the mobility of the polymer chains, which resulted in an increase in v. Once v took the maximum at $t_w = 194$ s, v drastically decreased in stage (II). In stage (II), although both the value and change in $d[\log(Q)]/dt_w$ are very small, it is clear from Fig. 3 that Q gradually increases. In this region, $d\Xi/d\,t_w$ varies significantly, indicating that a phase separation process was in progress, which is different from that in stage (I). In this stage, we assume that the solvents diffused from the polymer-rich phase to the bath, causing shrinkage of the phase-separated structure, which results in negative $d\Xi/d\,t_w$. The decrease in v implies a reduction in the polymer mobility in the polymer-rich phase caused by solvent desorption. Eventually, in stage (III), both v and $d\Xi/d\,t_w$ asymptotically approached 0 at $t_w \approx 310$ s. These results indicate that the shrinkage was terminated by a decrease in the mobility of the polymer.

In stage (III), the change of v is almost terminated, and the averaged static and dynamic properties appear to be in a stable state. However, the temporal fluctuations of dynamics clearly exist as shown in Fig. 4(d), and such temporal fluctuations can include important information for the NIPS process. The temporal fluctuations of C_I have sometimes been discussed in relation to the spatial heterogeneity of dynamics, dynamic heterogeneity [19,20,46–49]. The fluctuation of C_I can be discussed quantitatively by its normalized variance [45],

$$\chi(q,t) = \frac{\left\langle C_I^2(q,t_1,t)\right\rangle_{t_1} - \langle C_I(q,t_1,t)\rangle_{t_1}^2}{\langle C_I(q,t_1,t=0)\rangle_{t_1}^2}. \tag{4}$$

The parameter χ exhibits a peak around the inflection point of $g^{(2)}(q,\ \tau)$, and the height of this peak is proportional to the variance of the characteristic relaxation time. The experimentally measured variance χ is affected by statistical noise owing to the use of a finite number of pixels n_p. Thus, we corrected the measured $\chi(q,t)$ by applying a correction procedure based on extrapolation, $1/n_p = 0$, as reported previously [50,51]. The calculated χ at $t_w = 314$–332 s is shown in Fig. 8. It shows a prominent peak at $t \approx 2.8$ s, indicating that there are significant fluctuations on this timescale. The large fluctuations were also observed in C_I at $t_w > 332$ s, as shown in Fig. S2 in the Supplemental Material [36]. Although it is difficult to evaluate using Eq. (4) due to the long timescale of the fluctuations exceeding 18 s, they suggest that there were significant fluctuations in stage (III) at $t_w > 332$ s. These results represent that even at the end of the NIPS process, there are significant dynamic fluctuations that settle down with t_w.

IV. CONCLUSIONS

We investigated the structure and dynamics in the NIPS process of cuprammonium cellulose solution immersed in aqueous acetone solution by an *in situ* XPCS measurement. Our findings revealed that NIPS occurs in two steps. The first step involves solvent absorption into the polymer-rich membrane, which increases the characteristic length obtained by the SAXS profiles and speeds up the dynamic fluctuation observed by the XPCS analysis. The second step is the solvent desorption process. In this step, the characteristic correlation lengths decrease, and the dynamic fluctuation slows down.

After this step, the solidification of the polymer phase is completed.

This complex NIPS process was first revealed by simultaneously observing both microscopic structural and dynamical changes. For more specific characterization of NIPS process, it is important to investigate the effects of coagulation conditions, such as the composition of the polymer solution and coagulation solution, on the structure and dynamics. Such a systematic study will be presented elsewhere as future works. NIPS is an important phenomenon during the manufacture of fibers and other polymeric industrial products; thus, the optimization of industrial processes through such analysis should become increasingly important in the future.

ACKNOWLEDGMENTS

The XPCS measurements were performed at SPring-8 BL03XU (Frontier Softmaterial Beamline, FSBL) with Proposals No. 2019B7251 and No. 2020A7201. This study was partially supported by JSPS KAKENHI Grant No. JP23H05403.

[1] N. Peng, N. Widjojo, P. Sukitpaneenit, M. M. Teoh, G. G. Lipscomb, T.-S. Chung, and J.-Y. Lai, Evolution of polymeric hollow fibers as sustainable technologies: Past, present, and future, Prog. Polym. Sci. **37**, 1401 (2012).

[2] G. R. Guillen, Y. Pan, M. Li, and E. M. v. Hoek, Preparation and characterization of membranes formed by nonsolvent induced phase separation: A review, Ind. Eng. Chem. Res. **50**, 3798 (2011).

[3] T. Hongo (nee Hirasaki), M. Inamoto, M. Iwata, T. Matsui, and K. Okajima, Morphological and structural formation of the regenerated cellulose membranes recovered from its cuprammonium solution using aqueous sulfuric acid, J. Appl. Polym. Sci. **72**, 1669 (1999).

[4] H. Iijima, M. Iwata, M. Inamoto, and K. Kamide, Phenomenological effects of solvent-casting conditions on pore characteristics of regenerated cellulose membranes, Polym. J. **29**, 147 (1997).

[5] I. Miyamoto, Y. Matsuoka, T. Matsui, M. Saito, and K. Okajima, Studies on structure of cuprammonium cellulose III. Structure of regenerated cellulose treated by cuprammonium solution, Polym. J. **28**, 276 (1996).

[6] S. Ide, Filter made of cuprammonium regenerated cellulose for virus removal: A mini-review, Cellulose **29**, 2779 (2022).

[7] H. E. Cook, Brownian motion in spinodal decomposition, Acta Metall. **18**, 297 (1970).

[8] J. T. Cabral and J. S. Higgins, Spinodal nanostructures in polymer blends: On the validity of the Cahn-Hilliard length scale prediction, Prog. Polym. Sci. **81**, 1 (2018).

[9] J. W. Cahn and J. E. Hilliard, Free energy of a nonuniform system. III. Nucleation in a two-component incompressible fluid, J. Chem. Phys. **31**, 688 (1959).

[10] H. Manzanarez, J. P. Mericq, P. Guenoun, J. Chikina, and D. Bouyer, Modeling phase inversion using Cahn-Hilliard equations—influence of the mobility on the pattern formation dynamics, Chem. Eng. Sci. **173**, 411 (2017).

[11] B. F. Barton, P. D. Graham, and A. J. McHugh, Dynamics of spinodal decomposition in polymer solutions near a glass transition, Macromolecules **31**, 1672 (1998).

[12] J. U. Garcia, T. Iwama, E. Y. Chan, D. R. Tree, K. T. Delaney, and G. H. Fredrickson, Mechanisms of asymmetric membrane formation in nonsolvent-induced phase separation, ACS Macro Lett. **9**, 1617 (2020).

[13] M. R. Cervellere, X. Qian, D. M. Ford, C. Carbrello, S. Giglia, and P. C. Millett, Phase-field modeling of non-solvent induced phase separation (NIPS) for PES/NMP/water with comparison to experiments, J. Membr. Sci. **619**, 118779 (2021).

[14] T. Ishigami, K. Nakatsuka, Y. Ohmukai, E. Kamio, T. Maruyama, and H. Matsuyama, Solidification characteristics of polymer solution during polyvinylidene fluoride membrane preparation by nonsolvent-induced phase separation, J. Membr. Sci. **438**, 77 (2013).

[15] M. Sutton, A review of x-ray intensity fluctuation spectroscopy, C. R. Phys. **9**, 657 (2008).

[16] O. Bikondoa, X-ray photon correlation spectroscopy for the characterization of soft and hard condensed matter, in *X-Ray and Neutron Techniques for Nanomaterials Characterization* (Springer, Berlin, 2016), pp. 95–156.

[17] A. Madsen, R. L. Leheny, H. Guo, M. Sprung, and O. Czakkel, Beyond simple exponential correlation functions and equilibrium dynamics in x-ray photon correlation spectroscopy, New J. Phys. **12**, 055001 (2010).

[18] A. Girelli, H. Rahmann, N. Begam, A. Ragulskaya, M. Reiser, S. Chandran, F. Westermeier, M. Sprung, F. Zhang, C. Gutt, and F. Schreiber, Microscopic Dynamics of Liquid-Liquid Phase Separation and Domain Coarsening in a Protein Solution Revealed by X-Ray Photon Correlation Spectroscopy, Phys. Rev. Lett. **126**, 138004 (2021).

[19] T. Hoshino, Y. Okamoto, A. Yamamoto, and H. Masunaga, Heterogeneous dynamics in the curing process of epoxy resins, Sci. Rep. **11**, 9767 (2021).

[20] T. Hoshino, S. Fujinami, T. Nakatani, and Y. Kohmura, Dynamical Heterogeneity near Glass Transition Temperature under Shear Conditions, Phys. Rev. Lett. **124**, 118004 (2020).

[21] F. Ehrburger-Dolle, I. Morfin, F. Bley, F. Livet, G. Heinrich, S. Richter, L. Piché, and M. Sutton, XPCS investigation of the dynamics of filler particles in stretched filled elastomers, Macromolecules **45**, 8691 (2012).

[22] K. J. Johnson, L. Wiegart, A. C. Abbott, E. B. Johnson, J. W. Baur, and H. Koerner, *In operando* monitoring of dynamic recovery in 3D-printed thermoset nanocomposites by XPCS, Langmuir **35**, 8758 (2019).

[23] A. Nogales and A. Fluerasu, X ray photon correlation spectroscopy for the study of polymer dynamics, Eur. Polym. J. **81**, 494 (2016).

[24] T. Hoshino, D. Murakami, Y. Tanaka, M. Takata, H. Jinnai, and A. Takahara, Dynamical crossover between hyperdiffusion and subdiffusion of polymer-grafted nanoparticles in a polymer matrix, Phys. Rev. E **88**, 032602 (2013).

[25] R. Hernández, A. Nogales, M. Sprung, C. Mijangos, and T. A. Ezquerra, Slow Dynamics of nanocomposite polymer aerogels as revealed by x-ray photocorrelation spectroscopy (XPCS), J. Chem. Phys. **140**, 024909 (2014).

[26] H. Masunaga, H. Ogawa, T. Takano, S. Sasaki, S. Goto, T. Tanaka, T. Seike, S. Takahashi, K. Takeshita, N. Nariyama *et al.*, Multipurpose soft-material SAXS/WAXS/GISAXS Beamline at SPring-8, Polym. J. **43**, 471 (2011).

[27] R.-J. Roe, *Methods of X-Ray and Neutron Scattering in Polymer Science* (Oxford University Press, New York, 2000).

28] P. Debye, H. R. Anderson, and H. Brumberger, Scattering by an inhomogeneous solid. II. The correlation function and its application, J. Appl. Phys. **28**, 679 (1957).

[29] P. Debye and A. M. Bueche, Scattering by an inhomogeneous solid, J. Appl. Phys. **20**, 518 (1949).

[30] S. Manley, H. M. Wyss, K. Miyazaki, J. C. Conrad, V. Trappe, L. J. Kaufman, D. R. Reichman, and D. A. Weitz, Glasslike Arrest in Spinodal Decomposition as a Route to Colloidal Gelation, Phys. Rev. Lett. **95**, 238302 (2005).

[31] T. Gibaud and P. Schurtenberger, A closer look at arrested spinodal decomposition in protein solutions, J. Phys.: Condens. Matter **21**, 322201 (2009).

[32] Y. Gao, J. Kim, and M. E. Helgeson, Microdynamics and arrest of coarsening during spinodal decomposition in thermoreversible colloidal gels, Soft Matter **11**, 6360 (2015).

[33] H. Tanaka, Unusual Phase Separation in a Polymer Solution Caused by Asymmetric Molecular Dynamics, Phys. Rev. Lett. **71**, 3158 (1993).

[34] H. Tanaka, Universality of Viscoelastic Phase Separation in Dynamically Asymmetric Fluid Mixtures, Phys. Rev. Lett. **76**, 787 (1996).

[35] H. Tanaka, Viscoelastic phase separation, J. Phys.: Condens. Matter **12**, R207 (2000).

[36] See Supplemental Material at http://link.aps.org/supplemental/10.1103/PhysRevMaterials.7.045605 for irradiation position dependence of structural parameters obtained from SAXS, additional two-time correlation functions, and fitting parameters for time correlation functions.

[37] G. Brown, P. A. Rikvold, M. Sutton, and M. Grant, Speckle from phase-ordering systems, Phys. Rev. E **56**, 6601 (1997).

[38] A. Malik, A. R. Sandy, L. B. Lurio, G. B. Stephenson, S. G. J. Mochrie, I. McNulty, and M. Sutton, Coherent X-Ray Study of Fluctuations during Domain Coarsening, Phys. Rev. Lett. **81**, 5832 (1998).

[39] O. Bikondoa, On the use of two-time correlation functions for x-ray photon correlation spectroscopy data analysis, J. Appl. Crystallogr. **50**, 357 (2017).

[40] H. Guo, S. Ramakrishnan, J. L. Harden, and R. L. Leheny, Connecting nanoscale motion and rheology of gel-forming colloidal suspensions, Phys. Rev. E **81**, 050401(R) (2010).

[41] O. Czakkel and A. Madsen, Evolution of dynamics and structure during formation of a cross-linked polymer gel, Europhys. Lett. **95**, 28001 (2011).

[42] M. Reiser, J. Hallmann, J. Möller, K. Kazarian, D. Orsi, L. Randolph, H. Rahmann, F. Westermeier, E. Stellamanns, M. Sprung, F. Zontone, L. Cristofolini, C. Gutt, and A. Madsen, Photo-controlled dynamics and transport in entangled wormlike micellar nanocomposites studied by XPCS, Macromolecules **55**, 8757 (2022).

[43] C.-H. Cheng, K. Kamitani, S. Masuda, K. Uno, N. Dechnarong, T. Hoshino, K. Kojio, and A. Takahara, Dynamics of matrix-free nanocomposites consisting of block copolymer-grafted silica nanoparticles under elongation evaluated through x-ray photon correlation spectroscopy, Polymer **229**, 124003 (2021).

[44] Y. Shinohara, H. Kishimoto, N. Yagi, and Y. Amemiya, Microscopic observation of aging of silica particles in unvulcanized rubber, Macromolecules **43**, 9480 (2010).

[45] B. Ruta, O. Czakkel, Y. Chushkin, F. Pignon, R. Nervo, F. Zontone, and M. Rinaudo, Silica nanoparticles as tracers of the gelation dynamics of a natural biopolymer physical gel, Soft Matter **10**, 4547 (2014).

[46] A. Duri and L. Cipelletti, Length scale dependence of dynamical heterogeneity in a colloidal fractal gel, Europhys. Lett. **76**, 972 (2006).

[47] D. Orsi, L. Cristofolini, G. Baldi, and A. Madsen, Heterogeneous and Anisotropic Dynamics of a 2D Gel, Phys. Rev. Lett. **108**, 105701 (2012).

[48] P. Kwasniewski, A. Fluerasu, and A. Madsen, Anomalous dynamics at the hard-sphere glass transition, Soft Matter **10**, 8698 (2014).

[49] K. Kanayama, T. Hoshino, and R. Yamamoto, Relation between dynamic heterogeneities observed in scattering experiments and four-body correlations, Phys. Rev. Res. **4**, L022006 (2022).

[50] A. Duri, H. Bissig, V. Trappe, and L. Cipelletti, Time-resolved-correlation measurements of temporally heterogeneous dynamics, Phys. Rev. E **72**, 051401 (2005).

[51] V. Trappe, E. Pitard, L. Ramos, A. Robert, H. Bissig, and L. Cipelletti, Investigation of q-dependent dynamical heterogeneity in a colloidal gel by x-ray photon correlation spectroscopy, Phys. Rev. E **76**, 051404 (2007).